APPENDIX

A permanent AIFM1-MIA40/CHCHD4 complex drives complex I assembly through efficient import of NDUFS5

Silja Lucia Salscheider[1#], Sarah Gerlich[1#], Alfredo Cabrera-Orefice[2#], Esra Peker[1], Robin Alexander Rothemann[1], Lena Maria Murschall[1], Yannik Finger[1], Karolina Szczepanowska[3,4], Zeinab Alsadat Ahmadi[2], Sergio Guerrero-Castillo[2], Alican Erdogan[1], Mark Becker[1], Muna Ali[1], Markus Habich[1], Carmelina Petrungaro[1], Nele Burdina[1], Guenter Schwarz[1,4,5], Merlin Klußmann[1], Ines Neundorf[1], David A. Stroud[6,7], Michael T. Ryan[6], Aleksandra Trifunovic[3,4,5], Ulrich Brandt[2,4,*], Jan Riemer[1,4,*]

#, equal contribution

1, Institute for Biochemistry, University of Cologne, 50674 Cologne, Germany

2, Radboud Institute for Molecular Life Sciences, Radboud University Medical Center 6525 GA Nijmegen, The Netherlands

3, Institute for Mitochondrial Diseases and Aging, Medical Faculty, University of Cologne, 50931 Cologne, Germany

4, Cologne Excellence Cluster on Cellular Stress Responses in Aging-Associated Diseases (CECAD), University of Cologne, 50931 Cologne, Germany.

5, Center for Molecular Medicine, University of Cologne, 50931 Cologne, Germany

6, Department of Biochemistry and Molecular Biology, Monash Biomedicine Discovery Institute, Monash University, 3800, Melbourne, Australia.

7, Present address: Department of Biochemistry and Molecular Biology, Bio21 Molecular Science and Biotechnology Institute, University of Melbourne, Parkville, 3052 Victoria, Australia

* address correspondence to

J.R.: jan.riemer@uni-koeln.de, +49-221-470-7306

U.B.: ulrich.brandt@radboudumc.nl, +31-24-36-67098

TABLE OF CONTENT

APPENDIX TABLES

APPENDIX FIGURES

Appendix Table S1. Cell lines

Cell line	Inserted plasmid	Gene	Tag (C-terminal)	Source
Flp-In T-REx-293 (Flp-In™ T-REx™ – 293 cell)	—	—	—	ThermoFisher, R78007
Flp-In T-REx-293-Mock	pcDNA5/FRT/TO	—	—	This work
Flp-In T-REx-293-MIA40	pcDNA5/FRT/TO	ORF MIA40 iso. 1	Strep	Petrungaro et al, Cell Metab 2015
Flp-In T-REx-293-MIA40 C53S	pcDNA5/FRT/TO	ORF MIA40 iso. 1 (T157►A)	Strep	Petrungaro et al, Cell Metab 2015
Flp-In T-REx-293-MIA40 C55S	pcDNA5/FRT/TO	ORF MIA40 iso. 1 (T163►A)	Strep	Petrungaro et al, Cell Metab 2015
Flp-In T-REx-293-MIA40 C4,C53S,C55S	pcDNA5/FRT/TO	ORF MIA40 iso. 1 (T10; T157; T163►A)	Strep	Petrungaro et al, Cell Metab 2015
Flp-In T-REx-293-MIA40.1	pcDNA3	ORF MIA40 iso. 1 (bp 1-142)	Myc, 6xHis	This work
Flp-In T-REx-293-MIA40.2	pcDNA3	ORF MIA40 iso.2 (bp 1-155)	Myc, 6xHis	This work
Flp-In T-REx-293-AIFM1$_{MTS}$-MIA40	pcDNA5/FRT/TO	AIFM1 (bp 1-102): ORF MIA40	Strep	This work
Flp-In T-REx-293- Δ1-40 MIA40	pcDNA5/FRT/TO	ORF MIA40 iso. 1 (bp 41-142)	Strep	This work
Flp-In T-REx-293-AIFM1$_{MTS}$-Δ1-40 MIA40	pcDNA5/FRT/TO	AIFM1 (bp 1-102): ORF MIA40 iso. 1 (bp 41-142)	Strep	This work
Flp-In T-REx-293-AIFM1	pcDNA5/FRT/TO	ORF AIFM1	HA	This work
HEK293T wild type	—	—	—	This work
HEK293T AIFM1 *KO*	—	Deletion of AIFM1	—	This work
HEK293T AIFM1 *KO*-AIFM1	pcDNA5/FRT/TO	ORF AIFM1	HA	This work
HEK293T AIFM1 *KO*-Mock	PB-CuO-MCS-IRES-GFP-EF1-CymR-Puro	—	—	This work
HEK293T AIFM1 *KO*-AIFM1	PB-CuO-MCS-IRES-GFP-EF1-CymR-Puro	ORF AIFM1	—	This work
HEK293T AIFM1 *KO*-AIFM1	PB-CuO-MCS-IRES-GFP-EF1-CymR-Puro	ORF AIFM1	HA	This work

Cell line	Inserted plasmid	Gene	Tag (C-terminal)	Source
HEK293T wild type-Mock	PB-CuO-MCS-IRES-GFP-EF1-CymR-Puro	—	—	This work
HEK293T NDUFS5 *KO*	—	Partial deletion of NDUFS5	—	Stroud et al, Nature 2016
HEK293T AIFM1 *KO*-Δ1-40 MIA40	pcDNA5/FRT/TO	ORF MIA40 iso. 1 (bp 41-142)	Strep	This work
HEK293T AIFM1 *KO*-MIA40	pcDNA5/FRT/TO	ORF MIA40 iso. 1	Strep	This work
HEK293T AIFM1 *KO*-$AIFM1_{MTS}$-MIA40	pcDNA5/FRT/TO	AIFM1(bp 1-102): ORF MIA40	Strep	This work
HEK293T AIFM1 *KO*-$Smac_{MTS}$-MIA40	pcDNA5/FRT/TO	Smac (bp 1-59): ORF MIA40	Strep	This work
HEK293T AIFM1 *KO*-NDUFS5	PB-CuO-MCS-IRES-GFP-EF1-CymR-Puro	ORF NDUFS5	Strep	This work
HEK293T AIFM1 *KO*-NDUFA8	PB-CuO-MCS-IRES-GFP-EF1-CymR-Puro	ORF NDUFA8	Strep	This work
HEK293T AIFM1 *KO*-NDUFB10	PB-CuO-MCS-IRES-GFP-EF1-CymR-Puro	ORF NDUFB10	Strep	This work
HEK293T MIA40/CHCHD4 KD	—	Partial deletion of MIA40/CHCHD4	—	Murschall et al, BMC Biol 2020

Appendix Table S2. Primers

Primer	Sequence (5'-3' end)	Restriction site
AIFM1 fwd. for PB-CuO-MCS-IRES-GFP-EF1-CymR-Puro	GCTTCGAAGGCATGTTCCGGTGTGGAG	Bsp119I
AIFM1-HA rev. for PB-CuO-MCS-IRES-GFP-EF1-CymR-Puro	CCGCGGCCGCTCAAGCGTAATCTGGAACATCGTATGGGTAGTCTTCATGAATGTTG	NotI
AIFM1 rev. for PB-CuO-MCS-IRES-GFP-EF1-CymR-Puro	CCGCGGCCGCTCAGTCTTCATGAATGTTG	NotI
NDUFS5-Strep fwd. for PB-CuO-MCS-IRES-GFP-EF1-CymR-Puro	GATCCGCTAGC AACATGCCTTTCTTGGACATCCAG	NheI
NDUFS5-Strep rev. for PB-CuO-MCS-IRES-GFP-EF1-CymR-Puro	CGGCGGCCGCTTATTTCTCAAATTGTGGATGACTCCAGCTACCAGGCCGAGGCTCCCCCTTG	NotI
NDUFA8-Strep fwd. for PB-CuO-MCS-IRES-GFP-EF1-CymR-Puro	GATCCGCTAGCAACATGCCGGGGATAGTGGAGCTGC	NheI
NDUFA8-Strep rev. for PB-CuO-MCS-IRES-GFP-EF1-CymR-Puro	CGGCGGCCGCTTATTTCTCAAATTGTGGATGACTCCAGCTACCCTTGGTCCAGAAATAAAAGCGGCTGC	NotI
NDUFB10-Strep fwd. for PB-CuO-MCS-IRES-GFP-EF1-CymR-Puro	GATCCGCTAGCAACATGCCGGACAGCTGGGACAAGG	NheI
NDUFB10-Strep rev. for PB-CuO-MCS-IRES-GFP-EF1-CymR-Puro	CGGCGGCCGCTCATTTCTCAAATTGTGGATGACTCCAGCTACCGGAGGTGGCAGCGGCGGC	NotI

Appendix Table S3. siRNAs

siRNA	Target	Source	Identifier
Hs_ AIFM1_11	human AIFM1	*Qiagen*	SI02662114
Hs_ AIFM1_12	human AIFM1	*Qiagen*	SI02662653
Hs_ CHCHD4_ 5	human MIA40	*Qiagen*	SI04197354
Hs_ CHCHD4_ 6	human MIA40	*Qiagen*	SI04292176
negative control, siRNA scrambled	non-silencing	*Qiagen*	001027281

Appendix Table S4. Antibodies

Antibody	Source	Identifier
anti-ALR, rabbit polyclonal	Fischer et al., Mol Biol Cell 2013	N/A
anti-AIFM1 (4E7), mouse monoclonal	ThermoFisher Scientific	Cat# MA5-15880, RRID:AB_11153781
anti-AIFM1 (H-300), rabbit polyclonal	Santa Cruz Biotechnology	Cat# sc-5586, RRID:AB_2224668
anti-AIFM1 (internal domain), rabbit polyclonal	Merck	AB16501
anti-AK2, rabbit polyclonal	Finger et al., 2020	N/A
anti-ATP5α, mouse monoclonal	Abcam	Cat# ab14748, RRID:AB_301447
anti-CHCHD2, rabbit polyclonal	Proteintech	Cat# 19424-1-AP, RRID:AB_10638907
anti-COX19, rabbit polyclonal	Fischer et al., Mol Biol Cell 2013	N/A
anti-HA, rabbit polyclonal	Sigma-Aldrich	Cat# SAB4300603, RRID:AB_10620829
anti-CPOX, rabbit polyclonal	St John's Laboratory	Cat# STJ23214
anti-LDH (H-10), mouse monoclonal	Santa Cruz Biotechnology	Cat# sc-133123, RRID:AB_2134964
anti-MIA40, rabbit polyclonal	Fischer et al., Mol Biol Cell 2013	N/A
anti-NDUFA8 (E-3), mouse monoclonal	Santa Cruz Biotechnology	Cat# sc-398098
anti-NDUFA8, rabbit polyclonal	Abcam	Cat# ab184952
anti-NDUFA9, mouse monoclonal	Thermo Fisher Scientific	Cat# 459100, RRID:AB_2532223
anti-NDUFB7, rabbit polyclonal	Abcam	Cat# ab188575
anti-NDUFB8, mouse monoclonal	Abcam	Cat# ab110242, RRID:AB_10859122
anti-NDUFB10, rabbit polyclonal	Abcam	Cat# ab196019
anti-NDUFS5, rabbit polyclonal	Abcam	Cat# ab179806
anti-NDUFS5, rabbit polyclonal	Abcam	Cat# ab188510
anti-NDUFV1, rabbit polyclonal	Proteintech	Cat# 11238-1-AP, RRID:AB_21490401
anti-PDH, mouse monoclonal	Santa Cruz Biotechnology	Cat# sc-377092; RRID:AB_2716767
anti-SDHA, mouse monoclonal	Abcam	Cat# ab14715, RRID:AB_301433
anti-Strep, mouse monoclonal	Abcam	Cat# ab184224
anti-VDAC1, mouse monoclonal	Abcam	Cat# ab14734, RRID:AB_443084
anti-mouse, goat – Affinity Pure, HRP Conjugate	ImmunoReagents	Cat# GtxMu-003-DHRPX
Antibody	**Source**	**Identifier**

anti-rabbit, goat – Affinity Pure, HRP Conjugate	ImmunoReagents	Cat# GtxRb-003-DHRPX
anti-rabbit, goat Alexa Fluor 488	Thermo Fisher Scientific	Cat# A-11008, RRID:AB_143165
anti-mouse, goat Alexa Fluor 488	Thermo Fisher Scientific	Cat# A-11001, RRID:AB_2534069
anti-NDUFB6, mouse monoclonal	Invitrogen	A21359
anti-NDUFS2, mouse monoclonal	Abcam	Ab96160
anti-UQCRC1, mouse monoclonal	Mol. Probes	459140
anti-NDUFB6, mouse monoclonal	Invitrogen	A21359
anti-MT-CO1 (COX1), mouse monoclonal	Mol. Probes	459600
anti-HSP60, mouse monoclonal	Stress Marq	SMC-110

APPENDIX FIGURES

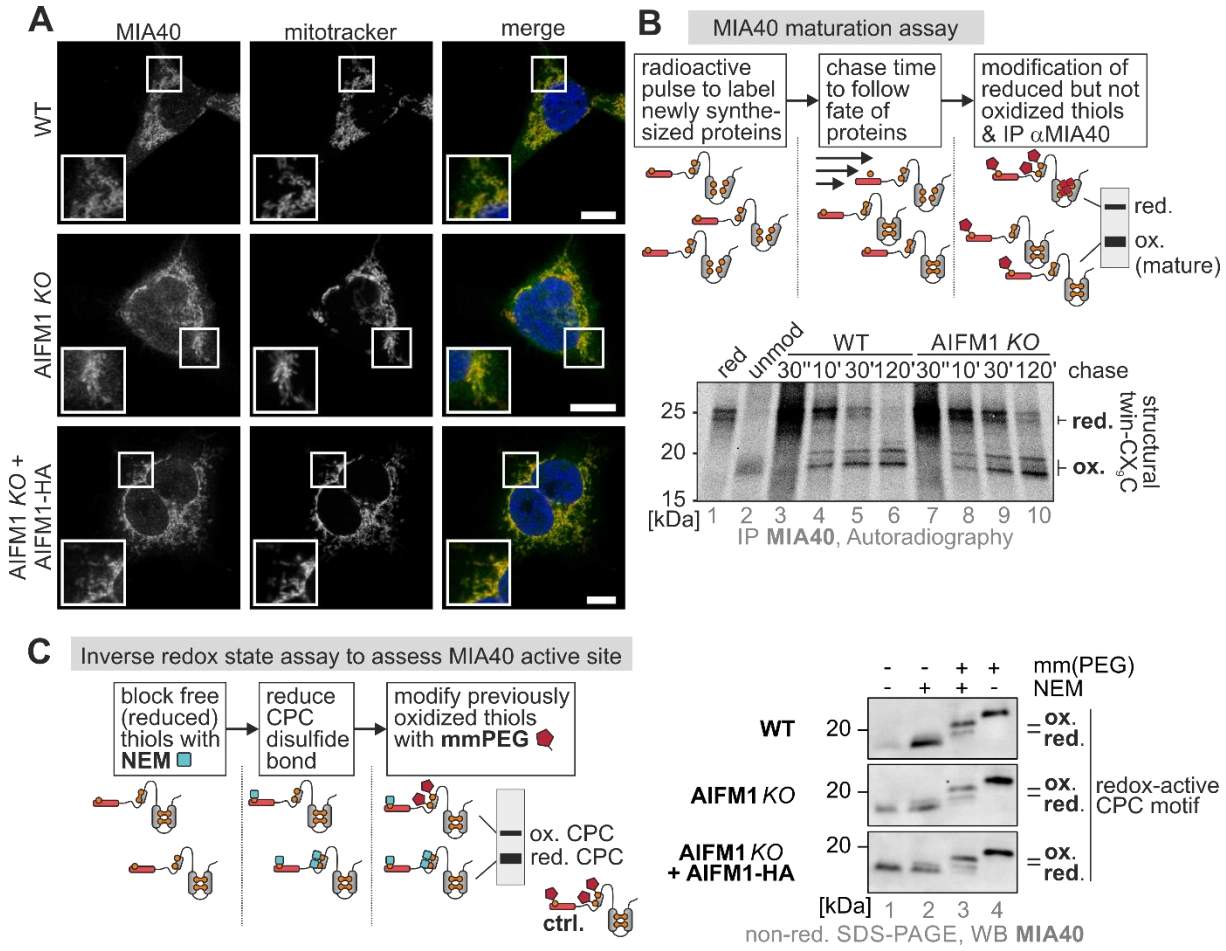

Appendix Figure S1 (related to Figure 1)**. MIA40 in AIFM1 knockout cells localizes to mitochondria, becomes oxidatively folded and has the correct redox state.**

A. Immunofluorescence analyses of MIA40 localization. HEK293 cells, AIFM1 knockout cells and AIFM1 knockout cells complemented with AIFM1-HA were analyzed by immunofluorescence staining against MIA40. Mitotracker served as mitochondrial control. Endogenous MIA40 colocalizes in all cell lines with the mitochondrial marker. bar, 10 µm

B. Oxidation kinetics of endogenous MIA40 in wild type and AIFM1 knockout cells. Wild type and AIFM1 knockout cells were subjected to pulse-chase analyses. Cells were pulse-labeled with [^{35}S]-methionine for 5 min. Subsequently, cells were chased for the indicated times. Then, cells were lysed and rapidly acidified by the addition of trichloroacetic acid (TCA). TCA pellets were dissolved and thiols modified with the maleimide compound mmPEG12. Thereby reduced (red.) thiols (total of 7 in MIA40) are modified and oxidized ones (ox., disulfide bonds) are not modified. Consequently, proteins containing mmPEG12-modified thiols migrate slower on SDS-PAGE. After mmPEG12 modification endogenous MIA40 was precipitated and analyzed by SDS-PAGE and autoradiography. Oxidation of the structural twin CX$_9$C motif is slightly delayed in AIFM1 knockout cells compared to wild type.

C. Redox state analyses of endogenous MIA40. Cell lines from **(a)** were subjected to an inverse redox state assay (Erdogan et al, Redox Biol 2017) to determine the redox

state of the redox-active CPC motif of MIA40. Intact cells are first exposed to N-ethyl maleimide (NEM) treatment to freeze the redox state and block all reduced cysteines. After NEM removal, cells are lysed and previously oxidized cysteines (*i.e.* in disulfide bonds) are reduced using tris(2-carboxyethyl)phosphine (TCEP). Cysteines are then modified with mmPEG12. Using this assay, cysteines that in the cell were present in a disulfide bond will be modified by mmPEG12, while cysteines that were previously reduced will be modified by NEM. Consequently, proteins containing previously oxidized cysteines will migrate slower on SDS-PAGE. Steady states of endogenous MIA40 are presented in lane 3 and are similar between all cell lines.

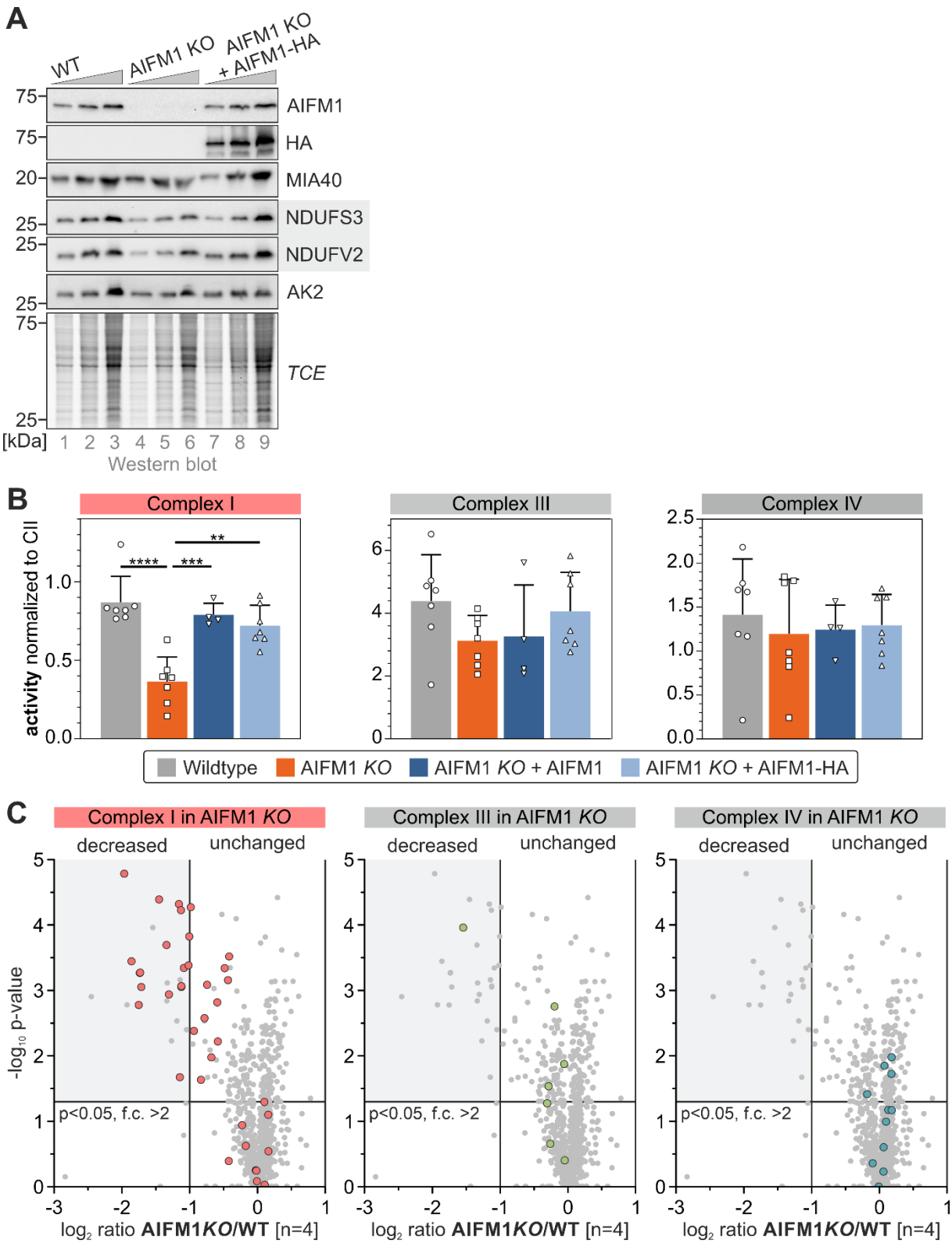

Appendix Figure S2 (related to Figure 1)**. Knockout of AIFM1 results in an isolated complex I deficiency.**

A. Assessment of protein levels in HEK293 cells, AIFM1 knockout cells and AIFM1 knockout cells with reintroduced AIFM1-HA (expression of AIFM1-HA induced for 3 days). This immunoblot shows additional subunits of complex I compared to **Figure 1D**. Different amounts of lysates from the indicated cells were analyzed by reducing

SDS-PAGE and immunoblotting. While levels of MIA40 were largely unchanged, levels of additional complex I subunits were diminished in AIFM1 knockout cells.

B. Activity analyses of respiratory chain complexes I, III and IV in HEK293, AIFM1 knockout and AIFM1 knockout complemented with AIFM1-HA or AIFM1. Activities of complexes I, III and IV were assessed in broken mitochondrial membranes and normalized to the activity of complex II. In AIFM1 knockout cells, complex I shows a significantly decreased activity to about 30-40% of wild type cells, in line with a decrease of total complex I levels to about 30-40%. Thus, the specific activity of still assembled complex I in AIFM1 knockout cells was unchanged. Activities of complexes III and IV do not significantly differ between wild type and AIFM1 knockout. Complementation of AIFM1 knockout cells with both, AIFM1 or AIFM1-HA rescues activity of complex I. N = 4-7 biological replicates; error bars indicate SD and an unpaired, two-sided Student's t-test was applied (** = $p<0.01$, *** = $p<0.001$, **** = $p<0.0001$).

C. Proteomic analysis comparing respiratory chain protein levels in HEK293 and AIFM1 knockout mitochondria (same as **Figure 1B.**). Mitochondria from the SILAC labeled cells were subjected to proteomic analyses. Mainly levels of complex I subunits but not of complex III and IV subunits were significantly reduced in AIFM1 knockout cells compared to HEK293 cells. N = 4 biological replicates, an unpaired one-sample two-sided Student's t-test was applied ($p<0.05$, fold change >2).

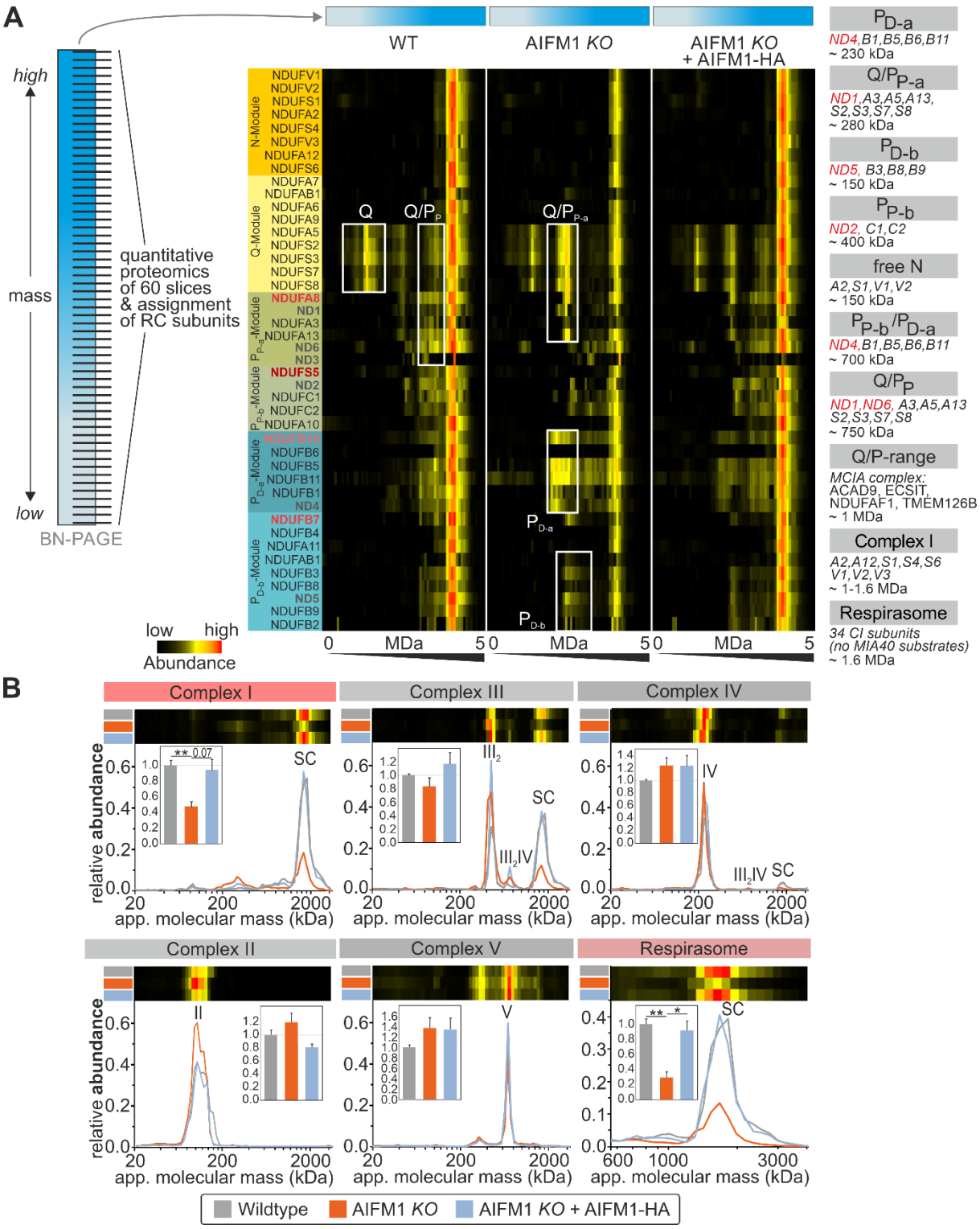

Appendix Figure S3 (related to Figure 2)**. Complexome profiling confirms the isolated complex I deficiency and specifically accumulating assembly intermediates in AIFM1 knockout.**

A. Representative overview heat maps of complete complexome profiles. The migration profiles of complex I subunits were arranged manually and color-coded by normalizing the relative abundance for each protein to the maximum value over all samples. Differences between wild type and AIFM1 knockout cells are already apparent at this stage of analysis. Positions of assembly intermediates are indicated.

Red, MIA40 substrates of complex I. Heat maps for 42 different subunits of complex I are shown, subunits ND4L and NDUFA1 are missing, because they were not detected by mass spectrometry. Note that NDUFAB1 is listed twice, because it is present in the Q- and the P_{D-b} module. The heat maps were calculated by averaging profiles from three biological replicates after alignment and abundance normalization to all detected mitochondrial proteins. Diagnostic subunits for each assembly intermediate/module are listed on the right (molecular weight and protein names omitting the preceding "NDUF").

B. Migration profiles of respiratory chain complexes in HEK293, AIFM1 knockout and AIFM1 knockout complemented with AIFM1-HA. Mitochondria isolated from the indicated cell lines were lysed in digitonin and analyzed by complexome profiling. Segments of averaged complexome profiles are shown as heat maps and plots to define the different respiratory chain complexes. Inserts show the relative abundances of each complex integrated over the entire mass range shown and normalized to the wildtype. Complex I and respirasome levels are significantly reduced to ~40% and ~30%, respectively. Consequently, complex III levels in the supercomplex are also reduced, while overall complex III levels (and levels of other respiratory chain complexes) were unchanged. N = 3 biological replicates, errors bars indicate SEM and an unpaired, two-sided Student's t-test was applied (* = $p<0.05$, ** = $p<0.01$).

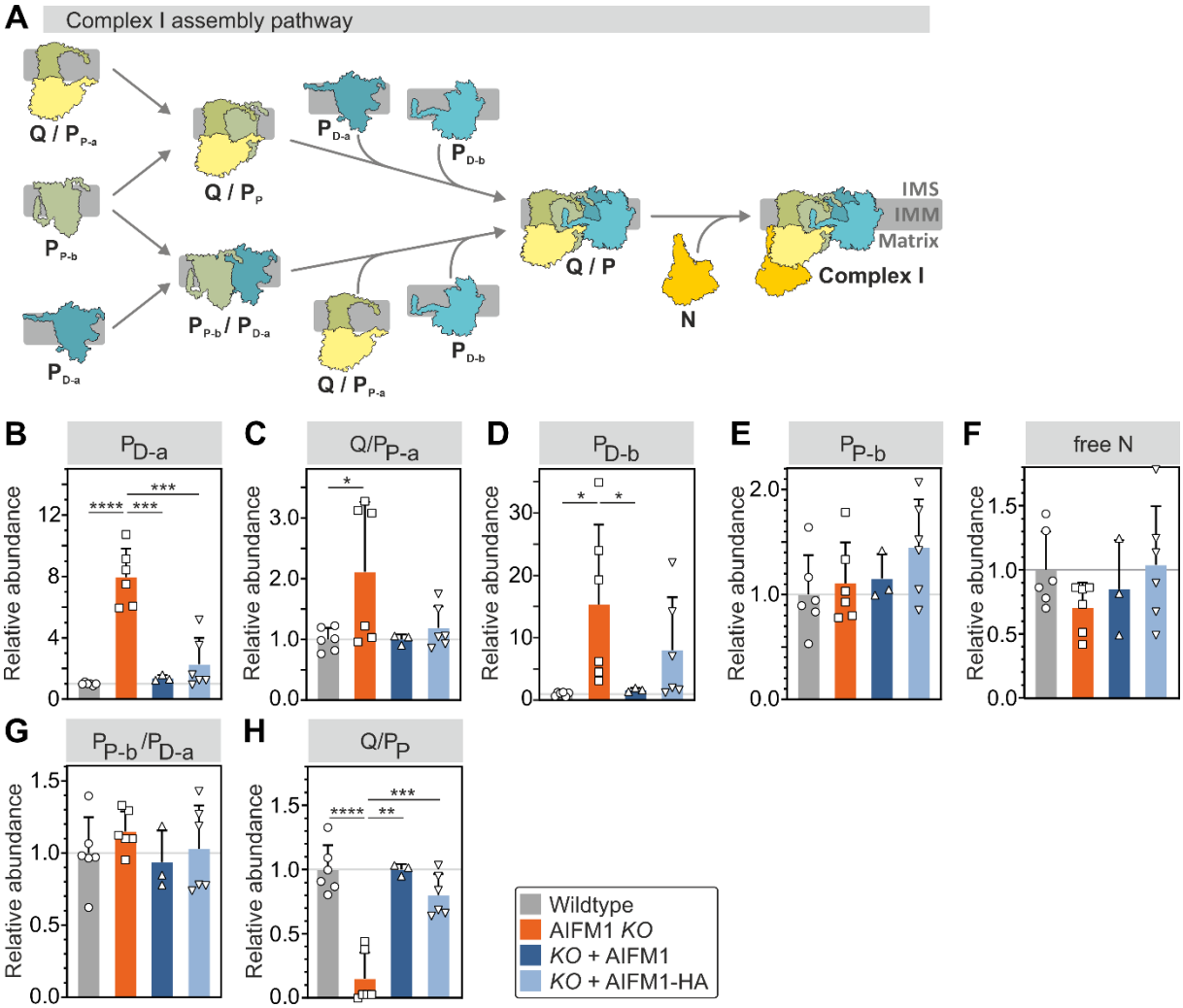

Appendix Figure S4 (related to Figure 2)**. Knockout of AIFM1 results in distinct changes in complex I assembly.**

A. The modular assembly pathway of complex I.

B-H. Detailed bar diagrams showing the amounts of the indicated assembly intermediates of complex I in HEK293, AIFM1 knockout and AIFM1 knockout complemented with AIFM1 or AIFM1-HA (data are the same as insets in **Figure 2A**). The relative abundances of diagnostic subunits for each module (see **Figure S3A**) were averaged in each slice, and areas under the curve around the indicated mass range were calculated and normalized to wild type (WT = 1). MIA40 substrates were excluded since changes in these subunits could be expected. Also excluded were NDUFAB1, because it occurs in two different modules, and those subunits that were below or too close to the detection limit in the respective intermediate. Since assembly intermediates $P_{P\text{-}b}/P_{D\text{-}a}$, Q/P_P and the free complex I were not fully separated due to similar masses, their abundances were assessed by averaging only subunits of the submodules unique for these intermediates in this mass range, *i.e.* $Q/P_{P\text{-}a}$, $P_{D\text{-}b}$ and N-module, respectively. In AIFM1 knockout cells, levels of the P_D-a (**B**), Q/P_P-a (**C**), P_D-b (**D**) assembly intermediates were increased. Levels of the $P_{P\text{-}b}$ (**E**), free N-module (**F**), and $P_{P\text{-}b}/P_{D\text{-}a}$ (**G**) were not significantly changed between the four analyzed cell lines. Levels of Q/P_P (**H**) was decreased in AIFM1 knockout cells. These findings indicate dramatic changes in complex I assembly in AIFM1 *KO* cells and point to

specific stalling points. N = 6 biological replicates, except AIFM1 *KO* + AIFM1 (N = 3); error bars indicate SD and an unpaired, two-sided Student's t-test was applied (* = $p<0.05$, ** = $p<0.01$, *** = $p<0.001$, **** = $p<0.0001$).

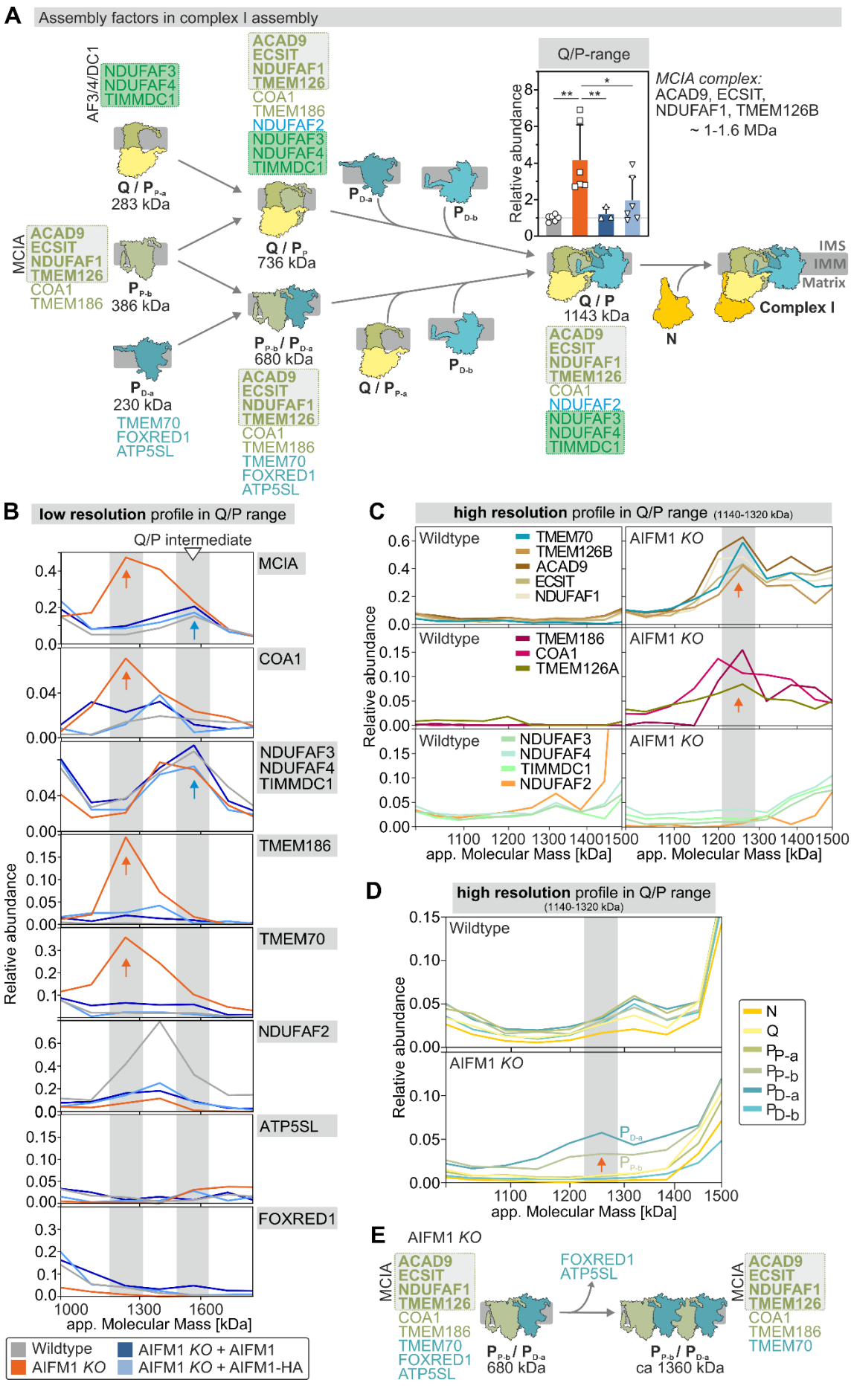
A
Assembly factors in complex I assembly
AF3/4/DC1
NDUFAF3
NDUFAF4
TIMMDC1
Q / P P-a
283 kDa
MCIA
ACAD9
ECSIT
NDUFAF1
TMEM126
COA1
TMEM186
P P-b
386 kDa
P D-a
230 kDa
TMEM70
FOXRED1
ATP5SL
ACAD9
ECSIT
NDUFAF1
TMEM126
COA1
TMEM186
NDUFAF2
NDUFAF3
NDUFAF4
TIMMDC1
Q / P P
736 kDa
P P-b / P D-a
680 kDa
ACAD9
ECSIT
NDUFAF1
TMEM126
COA1
TMEM186
TMEM70
FOXRED1
ATP5SL
P D-a
P D-b
Q / P P-a
P D-b
Q/P-range
Relative abundance
MCIA complex:
ACAD9, ECSIT,
NDUFAF1, TMEM126B
~ 1-1.6 MDa
Q / P
1143 kDa
ACAD9
ECSIT
NDUFAF1
TMEM126
COA1
NDUFAF2
NDUFAF3
NDUFAF4
TIMMDC1
N
IMS
IMM
Matrix
Complex I
B
low resolution profile in Q/P range
Q/P intermediate
MCIA
COA1
NDUFAF3
NDUFAF4
TIMMDC1
TMEM186
TMEM70
NDUFAF2
ATP5SL
FOXRED1
Relative abundance
app. Molecular Mass [kDa]
Wildtype
AIFM1 KO
AIFM1 KO + AIFM1
AIFM1 KO + AIFM1-HA
C
high resolution profile in Q/P range (1140-1320 kDa)
Wildtype
AIFM1 KO
TMEM70
TMEM126B
ACAD9
ECSIT
NDUFAF1
TMEM186
COA1
TMEM126A
NDUFAF3
NDUFAF4
TIMMDC1
NDUFAF2
Relative abundance
app. Molecular Mass [kDa]
D
high resolution profile in Q/P range
(1140-1320 kDa)
Wildtype
AIFM1 KO
N
Q
P P-a
P P-b
P D-a
P D-b
Relative abundance
app. Molecular Mass [kDa]
E
AIFM1 KO
MCIA
ACAD9
ECSIT
NDUFAF1
TMEM126
COA1
TMEM186
TMEM70
FOXRED1
ATP5SL
P P-b / P D-a
680 kDa
FOXRED1
ATP5SL
P P-b / P D-a
ca 1360 kDa
MCIA
ACAD9
ECSIT
NDUFAF1
TMEM126
COA1
TMEM186
TMEM70

Appendix Figure S5 (related to Figure 2)**. Knockout of AIFM1 results in accumulation of an off-pathway $P_{P\text{-}b}/P_{D\text{-}a}$ dimer.**

A. Assembly factors in the assembly pathway of complex I. Note that at the transition from the Q/P module to fully assembly complex I, the N-module joins and all still attached assembly factors are release. Boxed, assembly factors that co-migrate. Gray box, MCIA; green box, NDUFAF3/4, TIMMDC1. Accumulation of MCIA in the Q/P range was observed in "normal" complexome profiling. This observation was further investigated using high-resolution complexome profiling (essentially performing additional proteomic analyses of additional individual slides in a more focussed range) focussing on the mass range between 1000 and 1500 kDa (**C,D**).

B. "Normal" complexome profiling focussing on complex I assembly factors (analyses of 6 gel slices between 1000 and 2000 kDa). Averaged migration profiles and heat maps of complex I assembly factors in the Q/P range between 1000 and ca 2000 kDa in HEK293, AIFM1 knockout and AIFM1 knockout cells complemented with AIFM1-HA or AIFM1. The MCIA assembly factors and COA1 undergo a shift to lower molecular mass indicating accumulation of a smaller complex distinct from Q/P in AIFM1 knockout. NDUFAF3, NDUFAF4 and TIMMDC1 are only present in the Q/P module also in AIFM1 knockout cells indicating that the Q/P module is still formed in AIFM1 knockout cells. TMEM70 and TMEM186 that are not part of the Q/P complex in wild type are also found in increased amounts and shifted to the lower molecular mass range. NDUFAF2 is decreased in wild type and complemented cells. The assembly factors ATP5SL an FOXRED1 were barely detected in the size range of the Q/P module and the novel intermediate. N = 3 biological replicates.

C. "High-resolution" complexome profiling focussing on complex I assembly factors (analyses of 9 gel slices between 1000 and 1500 kDa). Averaged migration profiles and heat maps of complex I assembly factors in the Q/P range between 1000 and ca 1500 kDa in HEK293, AIFM1 knockout and AIFM1 knockout cells complemented with AIFM1-HA or AIFM1. The MCIA assembly factors, COA1, TMEM70 and TMEM186 are increased in a peak between 1200 and 1300 kDa confirming accumulation of an intermediate that is distinct from and smaller than the "normal" Q/P module. N = 2 biological replicates

D. "High-resolution" complexome profiling focussing on complex I modules. Like (**C**) except that the focus was on subunits of individual modules in the range between 1200 and 1300 kDa. $P_{D\text{-}a}$ and $P_{P\text{-}b}$ are increased in this range. Their combined mass would normally be less than half this mass suggesting that both modules accumulate as dimer. N = 2 biological replicates

E. Model. Block in complex I assembly results in the accumulation of an off-pathway assembly intermediate, a $P_{P\text{-}b}/P_{D\text{-}a}$ dimer with associated assembly factors.

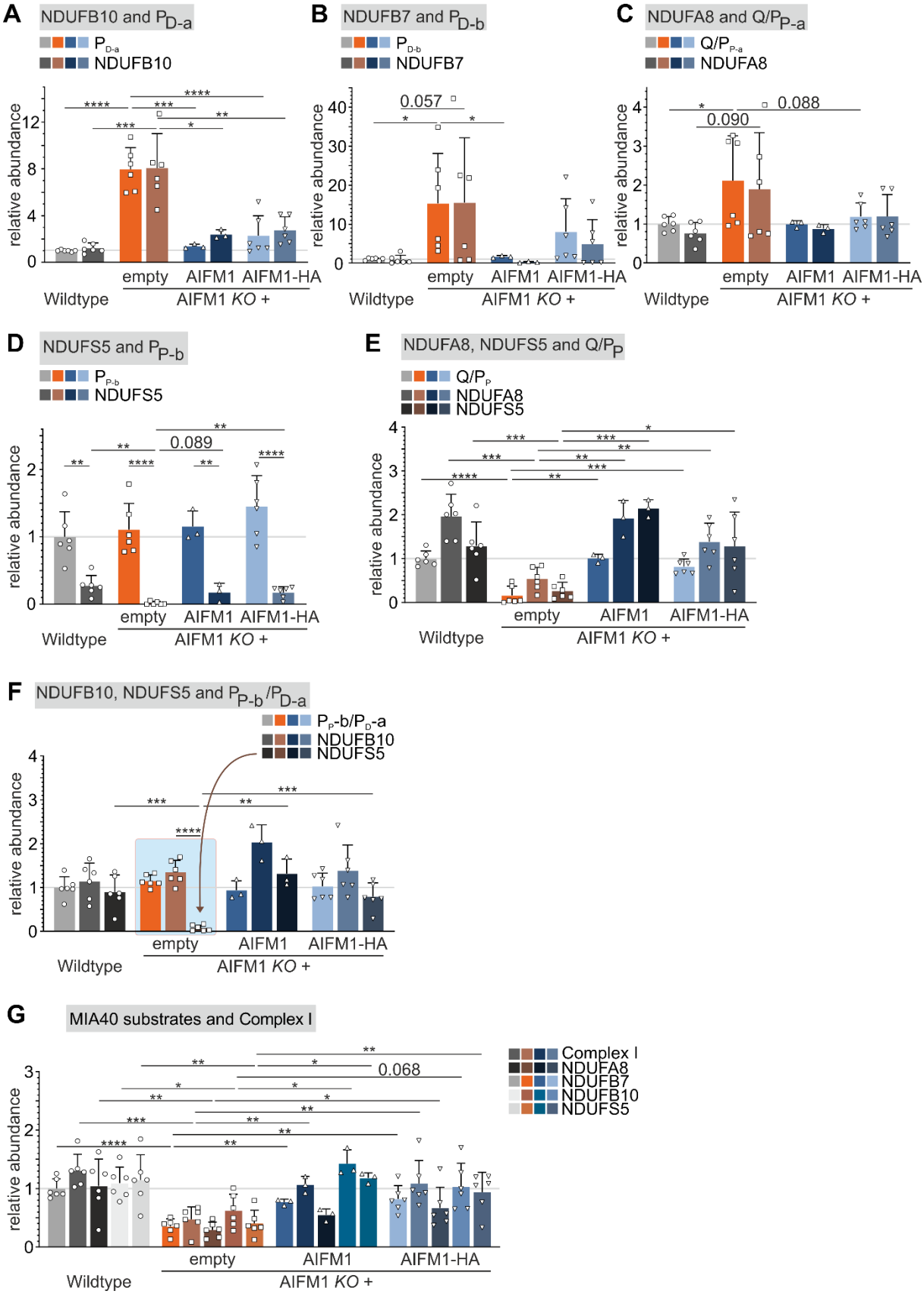
A
NDUFB10 and P D-a
P D-a
NDUFB10
relative abundance
Wildtype
empty
AIFM1
AIFM1-HA
AIFM1 KO +
B
NDUFB7 and P D-b
P D-b
NDUFB7
0.057
C
NDUFA8 and Q/P P-a
Q/P P-a
NDUFA8
0.088
0.090
D
NDUFS5 and P P-b
P P-b
NDUFS5
0.089
E
NDUFA8, NDUFS5 and Q/P P
Q/P P
NDUFA8
NDUFS5
F
NDUFB10, NDUFS5 and P P-b /P D-a
P P-b/P D-a
NDUFB10
NDUFS5
G
MIA40 substrates and Complex I
0.068
Complex I
NDUFA8
NDUFB7
NDUFB10
NDUFS5

Appendix Figure S6 (related to Figure 2)**. In AIFM1 knockout cells, NDUFS5 insertion during complex I assembly is impaired.**

A-G. Bar diagrams showing amounts of the indicated assembly intermediates of complex I and the four MIA40/CHCHD4 substrates that are part of complex I in HEK293, AIFM1 knockout and AIFM1 knockout complemented with AIFM1 or AIFM1-HA. Data are normalized to the wildtype assembly intermediates (WT = 1). MIA40/CHCHD4 substrates are presented together with the modules in which they occur. In AIFM1 *KO* cells, NDUFB10, NDUFA8 and NDUFB7 are increased with their respective initial assembly modules (**A-C**). In the $P_{P\text{-}b}$ module NDUFS5 is missing although it is associated with this module in the mature complex I (**D**). In the Q/P_P module, NDUFS5 and NDUFA8 are strongly decreased (**E**). Notably, NDUFS5 is missing from $P_{P\text{-}b}$ although the module is present at normal levels (**F,** same data as presented in **Figure 2C**). All substrates behave in mature complex I like the overall comlex, i.e. their levels are decreased to 30-40% of wildtype levels (**G**). N = 6 biological replicates, except AIFM1 *KO* + AIFM1 (N = 3); error bars indicate SD and an unpaired, two-sided Student's t-test was applied (* = $p<0.05$, ** = $p<0.01$, *** = $p<0.001$, **** = $p<0.0001$).

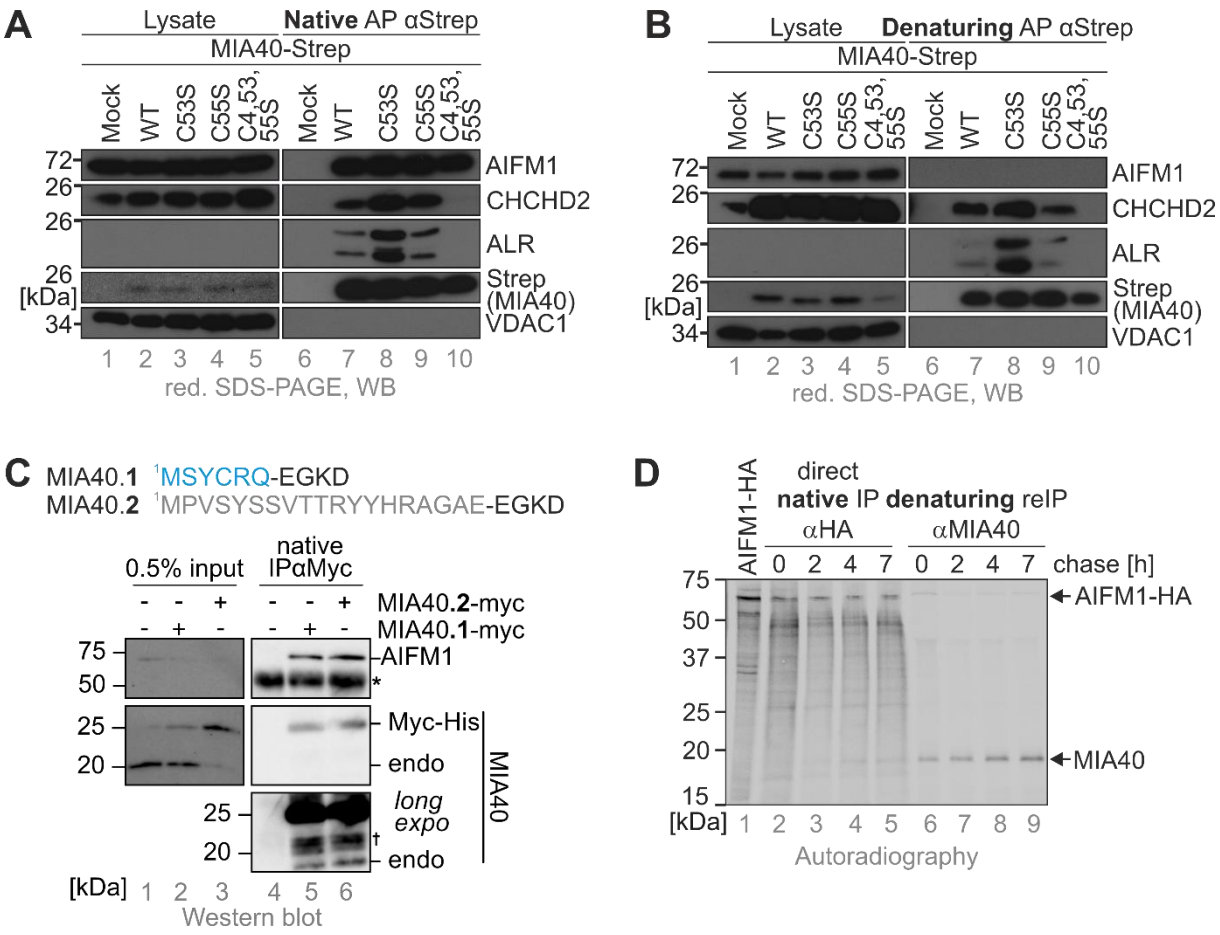

Appendix Figure S7 (related to Figure 4)**. AIFM1 and MIA40/CHCHD4 form a non-covalent long-lasting complex.**

A,B. Precipitation experiment to assess the interaction between AIFM1 and MIA40/CHCHD4. HEK293 cells stably expressing the indicated MIA40/CHCHD4-Strep variants were subjected to native (triton X100, **A**) or denaturing (SDS, **B**) affinity purification (AP) using streptactin beads. Precipitates were analysed by reducing SDS-PAGE and immunoblotting. All MAI40/CHCHD4 variants precipitated AIFM1 irrespective of their redox function in native but not denaturing immunoprecipitation.

C. Immunoprecipitation experiment to assess the interaction between AIFM1 and MIA40/CHCHD4. HEK293 cells stably expressing the two isoforms of MIA40/CHCHD4 as myc-tagged variants were subjected to native (triton X100) immunoprecipitation. Precipitates were analysed by reducing SDS-PAGE and immunoblotting. Both isoforms of MIA40/HCHD4 interact with AIFM1 despite differing in their N-terminal region.

D. Pulse chase analysis to assess the stability of the AIFM1/CHCHD4 complex. HEK293 cells stably expressing AIFM1-HA were subjected to pulse labelling with [^{35}S]-methionine for 10 min. Subsequently, cells were chased for the indicated times. Then, cells were lysed with triton X-100 and AIFM1-HA was precipitated by a native immunoprecipitation against the HA-tag. The resulting precipitate was subjected to denaturing immunoprecipitation against endogenous MIA40, and precipitates were analysed by SDS-PAGE and autoradiography. MIA40 coprecipitates with AIFM1 throughout the complete chase period.

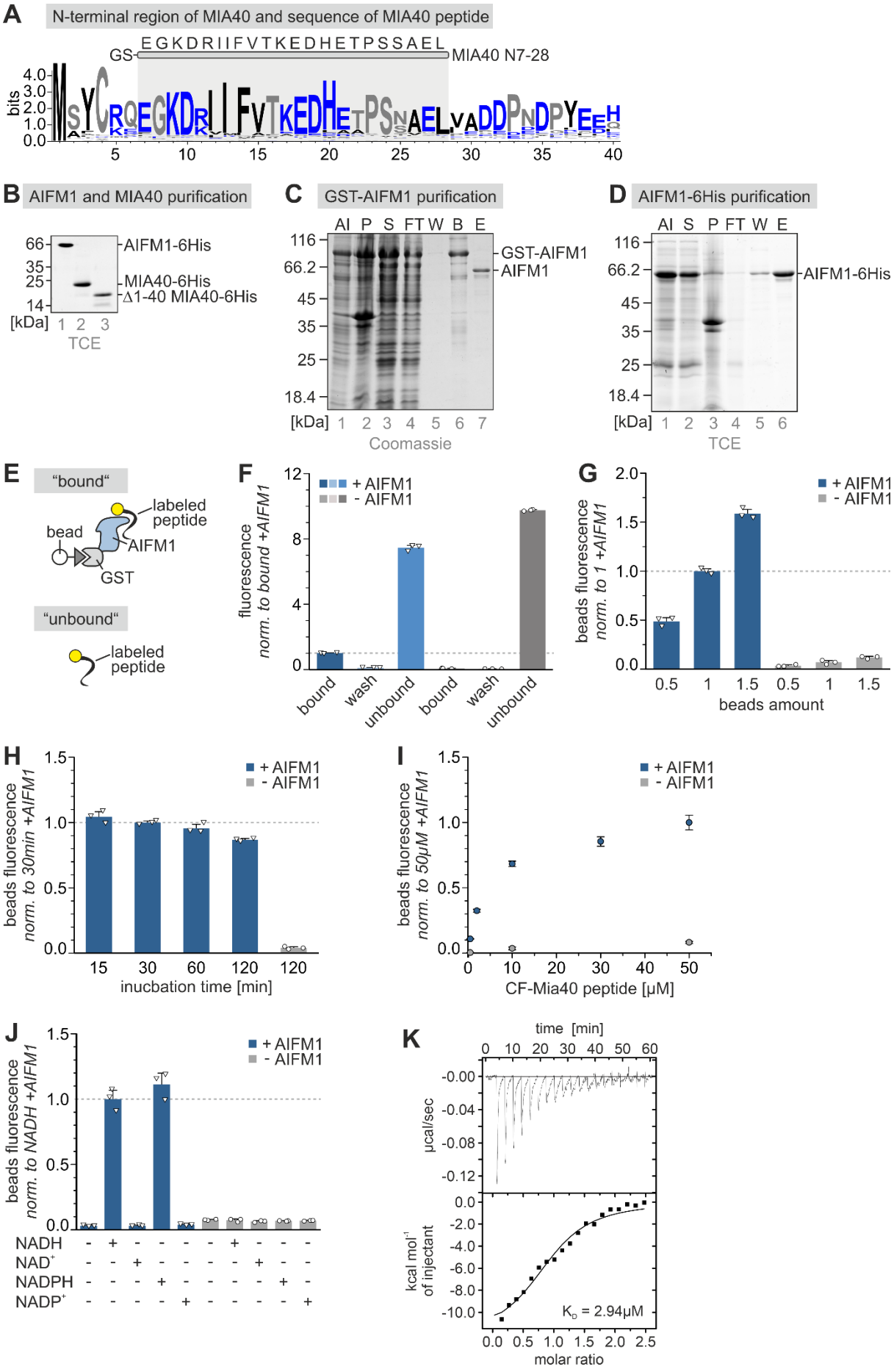
A
N-terminal region of MIA40 and sequence of MIA40 peptide
GS-EGKDRIIFVTKEDHETPSSAEL
MIA40 N7-28
bits
B
AIFM1 and MIA40 purification
AIFM1-6His
MIA40-6His
Δ1-40 MIA40-6His
[kDa]
TCE
C
GST-AIFM1 purification
Al P S FT W B E
GST-AIFM1
AIFM1
Coomassie
D
AIFM1-6His purification
Al S P FT W E
AIFM1-6His
TCE
E
"bound"
labeled peptide
bead
AIFM1
GST
"unbound"
labeled peptide
F
+ AIFM1
- AIFM1
fluorescence norm. to bound +AIFM1
bound
wash
unbound
G
beads fluorescence norm. to 1 +AIFM1
beads amount
H
beads fluorescence norm. to 30min +AIFM1
inucbation time [min]
I
beads fluorescence norm. to 50µM +AIFM1
CF-Mia40 peptide [µM]
J
beads fluorescence norm. to NADH +AIFM1
NADH
NAD+
NADPH
NADP+
K
time [min]
µcal/sec
kcal mol-1 of injectant
KD = 2.94µM
molar ratio

Appendix Figure S8 (related to Figure 4)**. *In vitro* analysis reveals a stable NAD(P)H-dependent interaction between AIFM1 and a peptide representing the N-terminal region of MIA40/CHCHD4.**

A. Peptide used for interaction studies with AIFM1. The chosen peptide represents a region with high conservation among different species. The N-terminal residues were left out during peptide design as they differ between the two isoforms of human MIA40/CHCHD4 that both can interact with AIFM1. The synthesized peptide was either left unlabelled or was labelled with 5,6-carboxyfluorescein. Blue, charged residues; larger letter font indicates conservation.

B-D. Purification of MIA40/CHCHD4-His, ∆1-40 MIA40/CHCHD4-His, GST-AIFM1 and AIFM1-His for binding studies between AIFM1 and MIA40/CHCHD4. The proteins were expressed in *E. coli* and purified by affinity purification. Eluates were loaded. AI, after induction; S, supernatant; P, pellet; FT, flow through; W, wash; E, eluate.

E-I. Establishment of the GST-AIFM1-bead peptide binding assay. Empty glutathione sepharose beads or beads loaded with GST-AIFM1 were used to establish the binding to a carboxyfluorescin (CF)-labelled fluorescent MIA40/CHCHD4 peptide (**E**). Beads were incubated with peptide in the presence or absence of NAD(P)H for 30 min at room temperature, they were then washed three times and bound peptide was assessed by fluorescence measurement with an excitation wavelength of 483 ± 7 nm and emission at 530 ± 15 nm. Peptide bound to glutathione sepharose beads only if AIFM1 was present. The peptide was present in excess for the assay so that the major part of the peptide remained in the unbound fraction after incubation with GST-AIFM1 beads (**F**). The chosen binding range allowed for semiquantitative analysis as changing amounts of beads led to linear changes in the amounts of peptide bound to the beads (**G**). Long binding times did not increase the amount of peptide bound to AIFM1-containg beads confirming 30 min of binding to be sufficient (**H**). Titration of peptide confirmed saturation of beads with peptide (**I**).

J. Performing the full binding assay between AIFM1 and MIA40/CHCHD4 fluorescent peptide demonstrated binding of the MIA40 peptide to AIFM1 in the presence of NADPH or NADH but not their oxidized counterparts.

K. ITC analysis of AIFM1 and unlabelled MIA40/CHCHD4 peptide. The partners bind to each other with a K_D of 2.94 µM. Data shown was normalized by the background signal of titrating MIA40/CHCHD4 peptide into buffer.

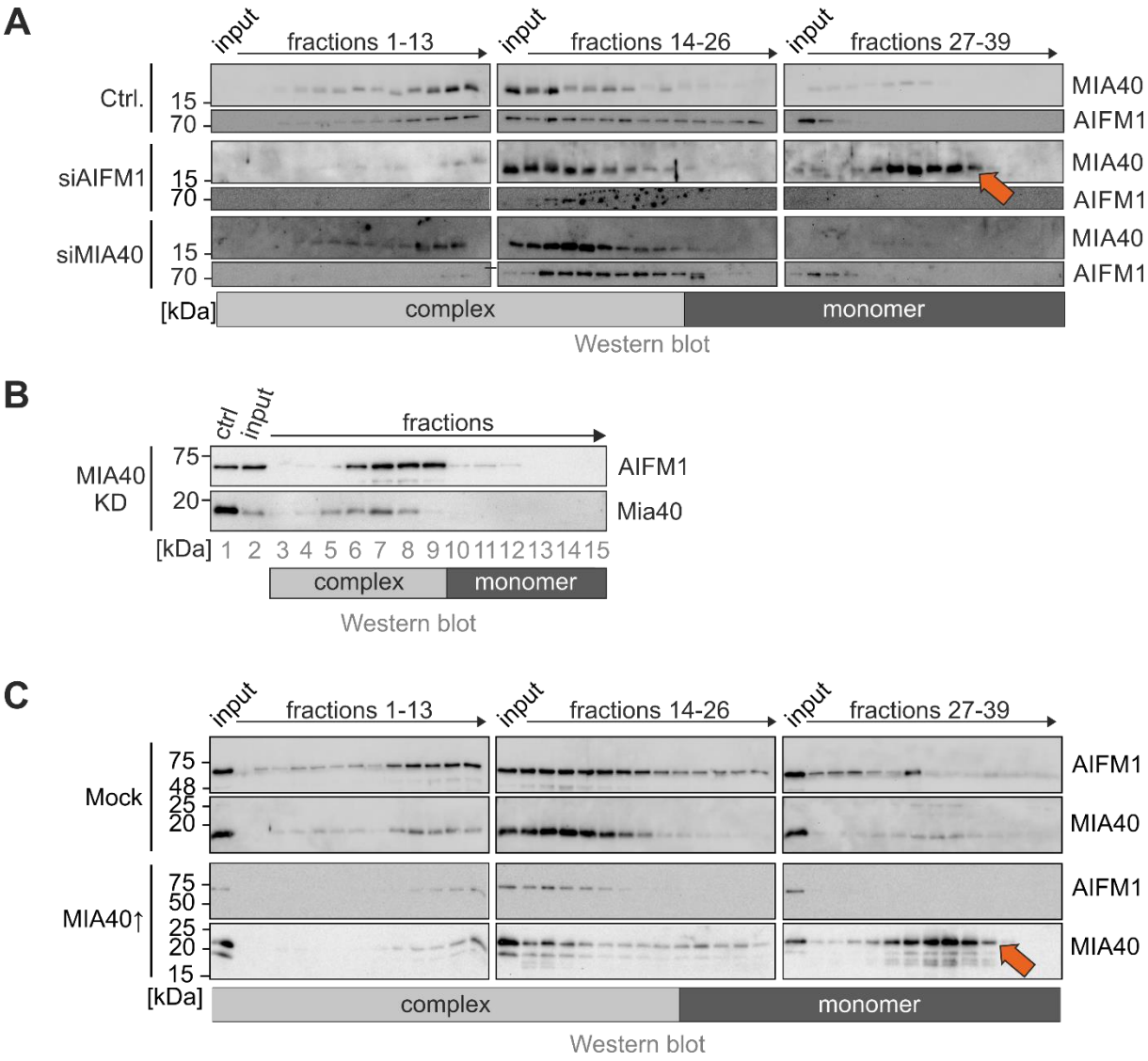

Appendix Figure S9 (related to Figure 5)**. The AIFM1-MIA40/CHCHD4 complex is stoichiometrically well balanced.**

A-C. Gel filtration analysis to assess the AIFM1-MIA40/CHCHD4 complex during siRNA-induced absence of one of the complex constituents in HeLa cells **(A)**, in HEK293 cells with permanently lowered levels of MIA40/CHCHD4 (generated by CRISPR-Cas9) (**B**), or during overexpression of MIA40/CHCHD4 in HEK293 cells **(C)**. Experiments were performed as described in **Figure 5A** except that MIA40/CHCHD4 or AIFM1 were depleted by siRNA treatment for 72 hours prior to the experiment or MIA40/CHCHD4 was inducibly overexpressed for 24 hours. SiRNA-mediated depletion of AIFM1 results in occurrence of monomeric MIA40 (orange arrow). Loss of MIA40 leads to a small shift of AIFM1. Overexpression of MIA40 results in occurrence of monomeric MIA40 (red arrow). Quantifications of these experiments are presented in **Figure 5C**.

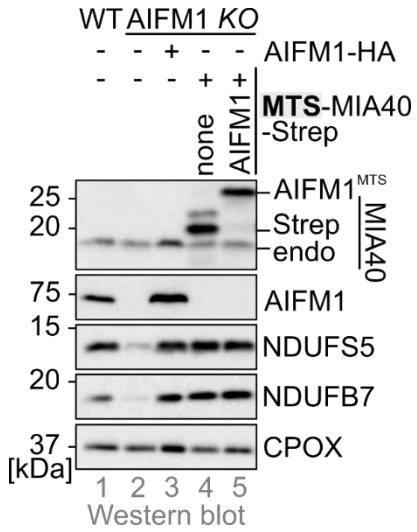

Appendix Figure S10 (related to Figure 6**). Re-expression of excess soluble or membrane-bound MIA40/CHCHD4 rescues loss of AIFM1**

Overexpression of MIA40/CHCHD4 or MTS-MIA40/CHCHD4 complements AIFM1 knockout cells. AIFM1 knockout cells expressing the indicated proteins were harvested and analyzed by reducing SDS-PAGE and immunoblot. In the absence of AIFM1, MIA40 substrates are diminished. This can be complemented by overexpression of AIFM1, MIA40/CHCHD4 or MTS-MIA40/CHCHD4. N = 2 biological replicates